



Analysis of gas-liquid two-phase flow field with six working teeth spiral incremental cathode for deep special-shaped hole in ECM

Jianli Jia¹ · Yougui Wei¹ · Baoji Ma¹ · Jiang Xu¹ · Yajing Hao¹

Received: 20 July 2023 / Accepted: 27 May 2024 / Published online: 3 June 2024
© The Author(s), under exclusive licence to Springer-Verlag London Ltd., part of Springer Nature 2024

Abstract

Screw drill is one of the most widely used power drilling tools in the field of deep sea drilling because of its excellent performance such as low drilling speed, high torque, and strong overload capacity. However, it has the problems of complex internal structure and long processing stroke of screw drill stator. In this paper, the electrochemical machining (ECM) technology is used to solve the problem of internal spiral curved surface special-shaped deep hole machining. Firstly, the initial cathode structure with spirally increasing tooth surface of six machining teeth is designed, and the gas-liquid two-phase flow field model of the gap is established to simulate and analyze it. The simulation results show that the flow field distribution of the electrolyte in the machining gap is not uniform and the bubble concentration is high. Secondly, the initial cathode structure is optimized by adding different numbers of liquid-increasing grooves on the tooth surface of the machined tooth, and the gas-liquid two-phase flow field is simulated. The simulation results show that the cathode structure with four additional baths on each tooth surface results in a better overall flow of electrolyte in the machining gap, a flow rate of more than 3 m/s in the machining area, and a significant reduction in the concentration of electrolyte bubbles, with a reduced rate of 18.7% and a smaller distribution area for the highest bubble concentration, ensure the machining accuracy. Finally, the orthogonal experiment of 4 factors and 4 levels was designed, and the optimized processing parameters were obtained by gray correlation analysis method, that is, inlet pressure of 0.4 MPa, machining voltage of 11 V, duty cycle of 40%, and cathode feed rate of 0.9 mm/min, under which the deviation of the large end diameter of the deep special-shaped hole was 0.15 mm, the surface roughness of the inner wall of the hole was 0.487 μm . The data shows that this combination of processing parameters meets the production requirements of the product. The data shows that this combination of machining parameters meets the production requirements of the product. The COMSOL simulation method significantly shortens the research cycle and saves research costs.

Keywords Deep special-shaped hole · ECM · Six working teeth cathode · Simulation

1 Introduction

With the advancement of technology, newly deep special-shaped hole parts with high strength, hardness, and high value have emerged in more and more fields, such as the mold industry and precision CNC machining machine tools. But the depth, accuracy, and efficiency of deep-hole parts required to improve also make for shaped deep-hole machining technology has become a prominent challenge in modern manufacturing. The parts of cement machining products are

mainly large shaft parts; these parts include both concentric and eccentric holes, to solve the processing difficulties, complex movement, and deep hole machining chip removal and other aspects of the problem [1]. The machining of long deep holes in the main body of a smoking gun has to be optimized because the holes are deeper and the chip path through the deep hole is longer, which does not facilitate chip removal and can easily cause deflection and vibration during work, leading to a scrap of the part [2]. Complex deep-hole parts in aircraft are key components of aero-engines, and the quality of deep-hole machining directly affects the service performance and service life of aero-engines [3]. With the use of traditional machining technology for deep special-shaped hole processing, the tool vibration frequency is high, cutting force and machining process chip removal difficulties,

✉ Jianli Jia
jl_202@xatu.edu.cn

¹ School of Mechatronic Engineering, Xi'an Technological University, Xi'an 710021, P.R. China

so to use new processing methods for shaped hole processing, special machining methods such as EDM, ultrasonic machining, and electrochemical machining. However, compared to electrochemical machining, EDM can get better machining accuracy, but in the process will produce damage to the processing cathode, resulting in higher processing costs [4]. Ultrasonic machining is generally combined with other machining methods to form a composite machining method, which further improves the accuracy of the original base [5]. Compared with EDM and ultrasonic machining technology, the electrolytic machining process has the advantages of no cutting stress, high machining accuracy, good machining efficiency and a wide range of processing, and no loss of the processing cathode in the process [6, 7].

With the continuous improvement and development of electrolytic machining technology, more and more researchers have conducted in-depth discussions and research on it. Xurong et al. used electrolytic machining to machine curved holes, optimized the parameters, and verified experimentally that the surface roughness of the specimens met the requirements of engineering applications [8]. Tang et al. used a computer simulation-assisted cathode design method to solve the uneven gap distribution and flow problems existing in complex parts with multi-stage internal tapered holes in electrochemical machining [9]. Rahman et al. used electrochemical machining to drill deep micro-bores in H_2SO_4 electrolytes for difficult-to-machine materials, resulting in holes with accurate dimensions and good surface finish [10]. Kharis et al. used electrolytic machining methods in conjunction with a hybrid machining physical model and a correlation system within the machining gap for the machining of small-diameter deep holes [11]. Prakash et al. set up a process test based on response surface methodology (RSM) with a central combinatorial approach, based on the effect of each process parameter on the machining results, multi-objective optimization was carried out with the optimization objectives of material removal rate, radial overcut, surface roughness, and tool electrode wear, and roughness prediction was obtained with a small error rate by using the TLBO algorithm with the constraints of the surface roughness [12].

Compared to conventional processing and other unusual processing methods, the electrolytic machining is accompanied by a common influence of multiple factors in multiple fields, such as flow, electric, temperature, and bubble fields. When coupling multiple physical fields, problems in a single field can affect the stability of other fields and eventually lead to inaccurate prediction of the final forming results [13, 14]. Pratik et al. simulated and analyzed cylindrical, conical, and hemispherical tool cathodes to predict the shape of the working cavity, obtained the effect of various process variables on the shape accuracy of the cavity, and proposed

guidelines to improve the contouring accuracy of micro ECMs [15]. Chen et al. proposed a gas-liquid two-phase turbulence model and solved it using a weakly coupled iterative method to obtain numerical simulations of gas volume fraction, temperature, and conductivity at equilibrium because hydrogen gas is generated during electrochemical processing and has an effect on the conductivity of the electrolyte [16]. Shen et al. used COMSOL software to derive simulation and experimental measurement profile curves for conical holes with different tapers by setting different cathode feed rates and operating voltages and compared them with experimental results to verify the accuracy of the simulation [17]. Wang et al. proposed that the electrochemical processing of metal gratings with diamond-shaped holes can effectively improve the processing quality of diamond-shaped holes, but due to the special shape of diamond-shaped holes, there is a diagonal problem and the electrolyte will cause stray corrosion on the side walls, so the synchronization method of pulsed current and low-frequency oscillation is used to improve the flow field [18]. Tim et al. proposed a new approach to simulate anode dissolution for electrolytic processing using a constant mesh, which permits the modeling of complex dissolution processes by controlling the effective material parameters without calculating costly re-gridding, and which yields realistic results [19]. Yin et al. studied the effect of machining voltage, initial machining gap, and feed rate on the forming accuracy of hexagonal holes by coupling electric and flow fields [20]. Jia et al. used COMSOL simulation software to simulate the flow field process of deep-hole electrochemical processing and optimized the cathode based on the simulation results. The flow field distribution can be effectively improved, and the machining accuracy will be improved by using two sets of 1.5-mm diameter liquid-filled holes with a slope of 20° and an angle of 22.5° [21].

Compared to conventional deep hole machining, electrolytic machining of deep holes can cause problems such as uneven flow field distribution, more differences in electrode concentration in the machining area, the effect of bubbles from the reaction on machining accuracy, and unpredictable final forming results. In this paper, a cathode structure with six working teeth is designed to ensure a single machining process. The COMSOL simulation software is used to simulate the gas-liquid two-phase flow field of the gap model, and the number of cathode liquid increasing tanks is modified according to the simulation results to achieve the optimization effect. Finally, using the optimized cathode structure, the comprehensive matching of process parameters is realized by gray correlation analysis. The development cycle is shortened and the processing cost is reduced.

2 Cathode design

2.1 Analysis of the processing object

The deep special-shaped hole has an approximate hexagonal end face, a length of 96 mm, and a central width of 39.5 mm. The internal spiral structure of the deep special-shaped hole is 100-mm long, and its structure shown in Fig. 1. From the electrolytic machining process and the actual processing situation, the spiral processing special-shaped hole has a long processing process, processing parts of the material removal is extremely large, but the removal amount is not uniform characteristics. As a result of the spiral process, the tool cathodes are subjected to increased spin on the horizontal feed, which causes an uneven flow of electrolytes between the anode and cathode, resulting in severe short-circuiting and burning of the tool cathodes. The spiral process is, therefore, more complex than a single-directional feed process.

2.2 Electrode materials

The principle of electrolytic processing is the use of anode materials in the electrolyte produced by the anode dissolution reaction of a processing method, the main criteria for the selection of cathode materials are corrosion-resistant, conductive, and easy to process and repair, and the more commonly used cathode materials are brass, tungsten copper, and bronze. For the spiral deep-shaped hole structure processed in this paper, due to the large amount of material removal, the cathode needs to be corrosion-resistant, conductive, and easy to process the characteristics of this in a comprehensive comparison of the use of H62 brass has the highest value, and in the machining of the cathode surface of the surface of the part of the region using epoxy resin for insulation, the cathode is a good choice.

Fig. 1 Schematic diagram of the spiral form deep special-shaped hole structure

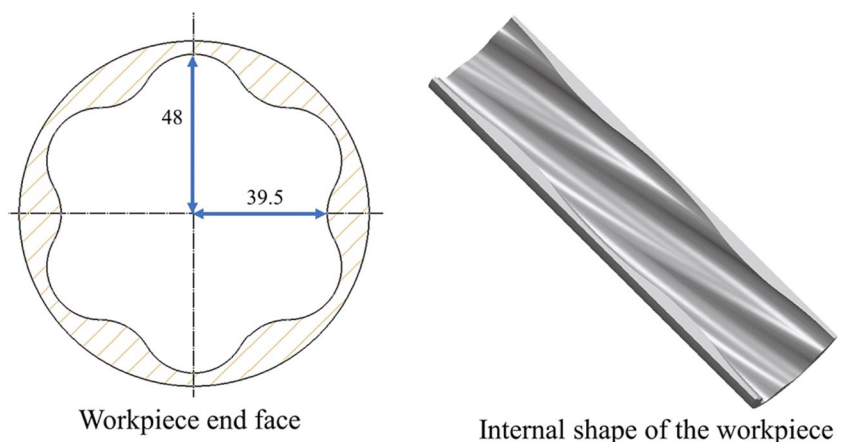


Table 1 Cathode material properties

Parameters	Values
Electric conductivity/(S·m ⁻¹)	1.56 × 10 ⁷
Heat capacity at constant pressure/(J·(kg·k) ⁻¹)	385
Density/(kg·m ⁻³)	8500
Thermal conductivity/(W·(m·k) ⁻¹)	116.7

The cathode material property settings in the simulation are shown in Table 1.

The anode material of the workpiece is 40CrNiMoV steel. 40CrNiMoV steel has high strength, toughness, and good hardenability and stability against overheating and is commonly used for high-strength shaft parts, connectors, and fasteners. The blank material of the workpiece is a bar with a prefabricated hole at the center of the bar, the elemental composition of the anode material is shown in Table 2, and the properties of the anode material in the simulation are set as shown in Table 3.

2.3 Design of the cathode structure

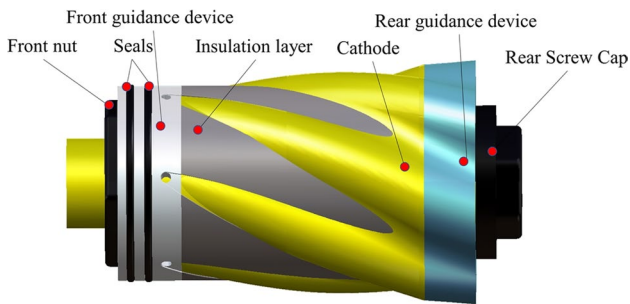
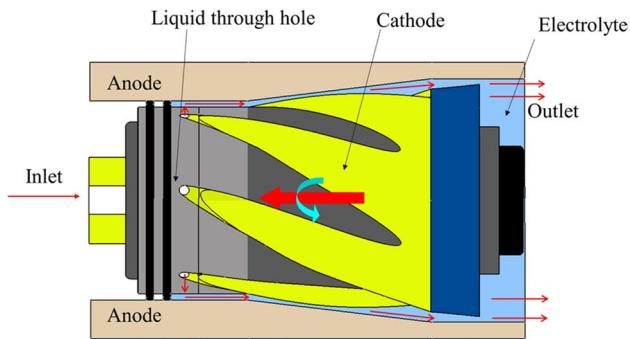
According to the characteristics of the deep special-shaped hole structure, this paper adopts a cathode structure with six working teeth, in which the front end of the working teeth is small, and the back end is large in a spiral increment so that the parts be processed can be processed and shaped at one time, as shown in Fig. 2. The small ends of the six working teeth are evenly distributed in the front of the cathode at the same angle, the insulating layer is placed between the working teeth, and the large ends of the working teeth are partially connected, with smooth transition at the connection, during the machining, the small end of the working teeth first rough the prefabricated hole to remove a large amount of part material, and then the large end of the working teeth finish the part to obtain a spiral-deep special-shaped hole that meets the requirements of forming accuracy.

Table 2 Chemical composition of 40CrNiMoV steel

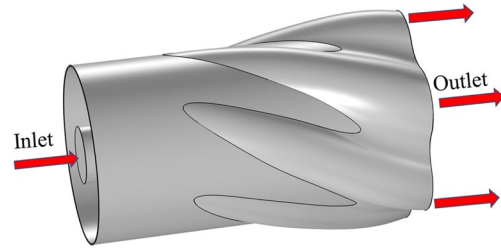
C	Si	Mn	Cr	Ni	Mo	Al	V	Nb	Ti
0.39	0.34	0.69	0.89	1.54	0.22	0.039	0.089	0.005	0.005

Table 3 Properties of workpiece anode materials

Parameters	Values
Electric conductivity/($S \cdot m^{-1}$)	1.12×10^7
Heat capacity at constant pressure/($J \cdot (kg \cdot K)^{-1}$)	440
Density/($kg \cdot m^{-3}$)	7830
Thermal conductivity/($W \cdot (m \cdot K)^{-1}$)	76.2

**Fig. 2** Schematic diagram of the cathode structure**Fig. 3** Electrolyte flow and cathode motion form and direction

This paper uses a cathode structure with a spiral progression of six working teeth surfaces. The electrolyte flows into the cathode through a hollow spiral rod feed device, with a rear nut seal at the end of the spiral rod to prevent the electrolyte from flowing out, and the electrolyte flows inside the cathode body through a through-hole and an increasing hole into the cathode teeth for machining and finally flows out through the rear guide part. The cathode rotates counterclockwise around the direction of the workpiece axis and moves along the axis in the opposite

**Fig. 4** Gap geometry model diagram

direction to the flow of electrolyte, Fig. 3 shows the flow of electrolyte and cathode movement form and direction.

3 Simulation of the gas-liquid two-phase flow field

3.1 Modeling the gap

The gap model for electrolytic machining in the machining equilibrium state, electrolyte in the tool cathode, the workpiece anode, and fixture in the flow of electrolyte existence of the spatial position model, in the three-dimensional software using Boolean operations can be obtained through a gap geometric model as shown in Fig. 4; the initial machining gap is taken as 0.5 mm.

3.2 Simulation mathematical modeling

3.2.1 Mathematical modeling of the gas-liquid two-phase flow field

To investigate the simulation results in the ideal state, as well as to facilitate the subsequent calculation, the simulation process of the machining gap is set up with the following two assumptions: 1, the fluid in the flow field is incompressible Newtonian fluid and 2, the use of the turbulent flow of electrolyte can quickly eliminate the electrolysis process in the cathode and anode parts of the electrolysis products on the electrode parts of the concentration of the impact. The energy loss generated by the electrolyte during processing is ignored and the flow of the electrolyte also satisfies the laws of conservation of mass and conservation of momentum. The motion of an incompressible fluid inside the ideal state assumption 1 satisfies the N-S equation:

$$\rho \frac{dV}{dt} = \rho \mathbf{g} - \nabla p + \mu \nabla^2 V \tag{1}$$

$$\nabla \cdot V = \frac{\partial u}{\partial x} + \frac{\partial v}{\partial y} + \frac{\partial \omega}{\partial z} = 0 \tag{2}$$

where ρ is the fluid density, u is the component of the vector velocity in the x -direction, p is the fluid micro circular pressure value, μ is the dynamic viscosity, g is the gravitational acceleration, ∇ is the gradient operator, ∇^2 is the Laplace operator, and $\nabla \cdot V$ is the volume expansion rate.

The flow state of a turbulent electrolyte is discriminated using the Reynolds number (Re):

$$Re = \frac{uD_h}{\nu} \tag{3}$$

where D_h is the hydrodynamic diameter and ν is the electrolyte kinematic viscosity.

In order to calculate the turbulent kinetic energy k and the turbulent dissipation rate ϵ , the standard $k-\epsilon$ model is used in this paper and the effect of gravity is neglected, the standard $k-\epsilon$ equation is as follows:

$$\rho_l \frac{\partial k}{\partial t} + \rho_l u_l \nabla k = \nabla \left[\left(\mu + \frac{\mu_T}{\sigma_k} \right) \nabla k \right] + P_k - \rho_l \epsilon + S_k \tag{4}$$

$$\rho_l \frac{\partial \epsilon}{\partial t} + \rho_l u_l \nabla \epsilon = \nabla \left[\left(\mu + \frac{\mu_T}{\sigma_\epsilon} \right) \nabla \epsilon \right] + \frac{\epsilon}{k} (C_{\epsilon 1} P_k + C_{\epsilon 2} S_k - C_{\epsilon 2} \epsilon) \tag{5}$$

where P_k and S_k are both generating terms, shear- and bubble-induced turbulence, respectively, expressed as follows:

$$P_k = \frac{\mu_T}{2} |\nabla u + (\nabla \mu)^T|^2 \tag{6}$$

$$S_k = -\beta C_k |\nabla p|^2 \tag{7}$$

The constants in the formula used are as follows: $C_{\epsilon 1} = 1.44$, $C_{\epsilon 2} = 1.92$, $\sigma_k = 1.0$, and $\sigma_\epsilon = 1.3$.

3.2.2 Simulation parameters

The simulation parameters used in this paper are shown in Table 4. To visualize the simulation results of the flow field and the gas-liquid two-phase field, the simulation results of the six-tooth cathode working area in the gap model are extracted for display, as shown in Fig. 5.

Table 4 Simulation parameters

Parameters	Numerical values
Electrolyte inlet pressure/(MPa)	0.4
Electrolyte outlet pressure/(Pa)	101,324
Electrolyte power viscosity/(Pa·s)	0.0008
Density of electrolyte/(kg·m ⁻³)	1100
Electrolyte conductivity/(S/m)	11.5
Gas diffusion coefficient/(mm ² /s)	5.19 × 10 ⁻³
Processing voltage/(V)	15
Workpiece anode material density/(kg/m ³)	7860
Molar mass of workpiece anode material/(kg/mol)	0.05585
Workpiece anode volume electrochemical equivalent/(cm ³ ·(A·min) ⁻¹)	0.0022

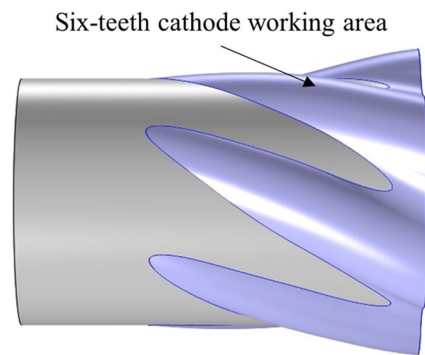


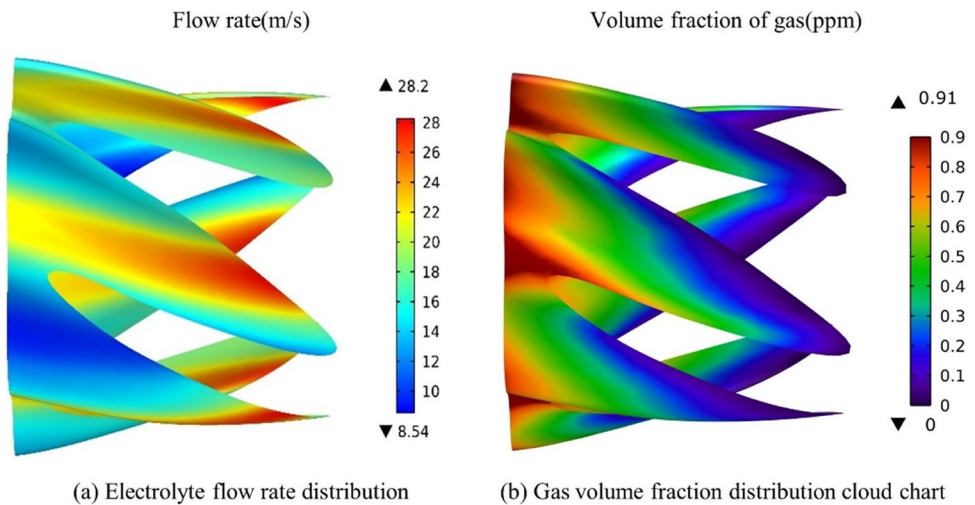
Fig. 5 Map of the six-tooth cathode working area

4 Simulation results analysis and discussion

4.1 Discussion of simulation results for the gas-liquid two-phase flow field of interstitial electrolytes

The distribution of electrolyte flow rate in the region of shaped deep hole machining is shown in Fig. 6a, from which it can be seen that the highest flow rate in the gap model reaches 28.2 m/s, while the flow rate at the top of the tooth and the tooth connection is smaller at 8.54 m/s. This phenomenon is due to the fact that the big end part of cathode machining working tooth is farther away from the position of the liquid injection hole, and electrolyte generates the kinetic loss in the process of flowing through the working tooth. The flow rate of electrolyte shows a decreasing trend. And when the electrolyte flows out from the liquid injection hole, from the small end of the cathode working tooth to the big end of the process, as the cross-sectional area of the electrolyte in the processing gap gradually increases, the flow rate of the electrolyte decreases with the cross-sectional area, especially in the

Fig. 6 The distribution cloud diagram of electrolyte flow rate and bubble concentration in the special-shaped deep hole processing area



big end of the cathode working tooth, the cross-sectional area of the electrolyte processing gap is the largest, and at this time, the electrolyte flowing out of the liquid injection hole cannot satisfy the demand of the electrolyte for the cross-sectional gap of the cathode working tooth at the big end of the cathode working tooth, which is prone to the phenomenon of short-circuit, and the machining process is not stable. Increasing liquid tank structure and processing of the small end of the tooth to the top of the tooth and the large end of the tooth part of the incremental form, the two add up to be more conducive to enhance the machining accuracy, so in order to meet the cathode working tooth machining gap in the sufficient electrolyte, this paper in the cathode designed to increase the liquid tank structure. The cloud diagram of the electrolyte bubble concentration distribution in the deep special-shaped hole machining area is shown in Fig. 6b, it can be seen that the distribution of the gap electrolyte bubbles is approximately the same as the flow field distribution, and it can be seen that the bubble distribution is mainly influenced by the flow field distribution. As seen in the figure, the volume fraction of gas is the highest at the top of the working tooth and the big end connection, up to 0.91. In actual processing, the gas concentration in the cathode and anode gap will have a direct effect on the conductivity, and a high gas concentration will reduce the conductivity of the electrolyte, which indirectly leads to a reduction in the rate of anode corrosion, so that the top of the working tooth and the big end connection of the material etching is lower, and the accuracy of the processed workpiece cannot be guaranteed. The precision of the workpiece cannot be guaranteed, and in serious cases, it may lead to collision between the anode of the workpiece and the processing cathode, which has an impact on the stability of processing. The cathode structure should be optimized to increase the flow rate of

the electrolyte at the top of the working teeth and the large end of the tooth connection.

4.2 Optimization of the cathode structure

Through the analysis of the simulation results of the initial structure, it can be seen that the electrolyte flow rate distribution in the initial structure is not uniform, and the method of designing the liquid increasing tank in the cathode structure can significantly improve the electrolyte flow rate from the small end to the large end of the cathode working tooth. With the increase of the overall flow rate of the electrolyte in the processing area, the stability of the electrolyte flow will become better, and the bubble concentration is low, the bubble distribution area is small, and the machining accuracy and quality of the workpiece can be effectively improved. Therefore, this paper decided to increase the liquid tank on the original structure to optimize the cathode structure. Four different types of cathode structure with different numbers of booster slots are designed for this purpose, as shown in Fig. 7, with structures 1, 2, 3, and 4 being the three-booster slot cathode structure, the four-booster slot cathode structure, the five-booster slot cathode structure, and the six-booster slot cathode structure respectively.

4.2.1 Analysis of flow field simulation results

The optimized electrolyte flow rate distribution cloud in the deep special-shaped hole machining area is shown in Fig. 8. It can be seen from the diagram that the optimized cathode structure shows a significant increase in the flow rate from the top of the working tooth to the end of the large tooth. This shows that the addition of the pressurized groove increases the electrolyte pressure from the top of the working tooth to the large end of the working tooth, and the

Fig. 7 Cathode structure for four different types with different number of baths for liquid enrichment

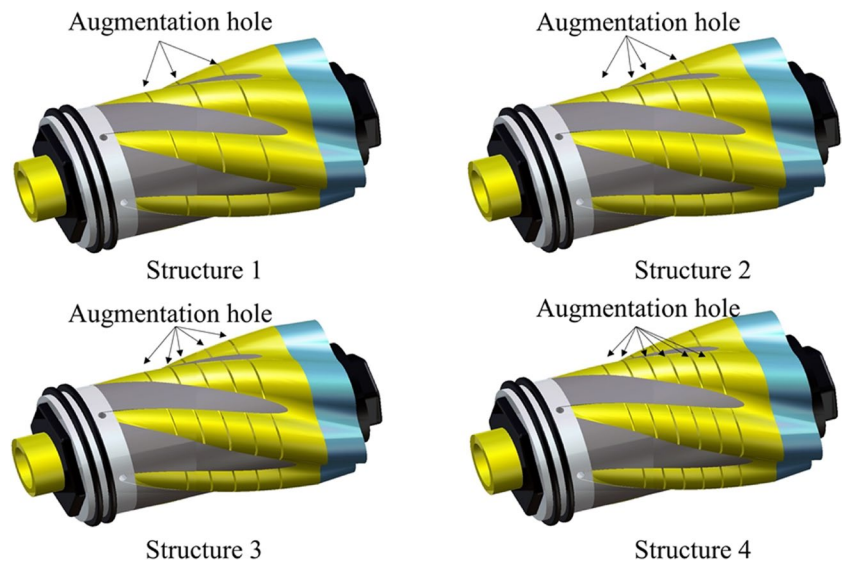
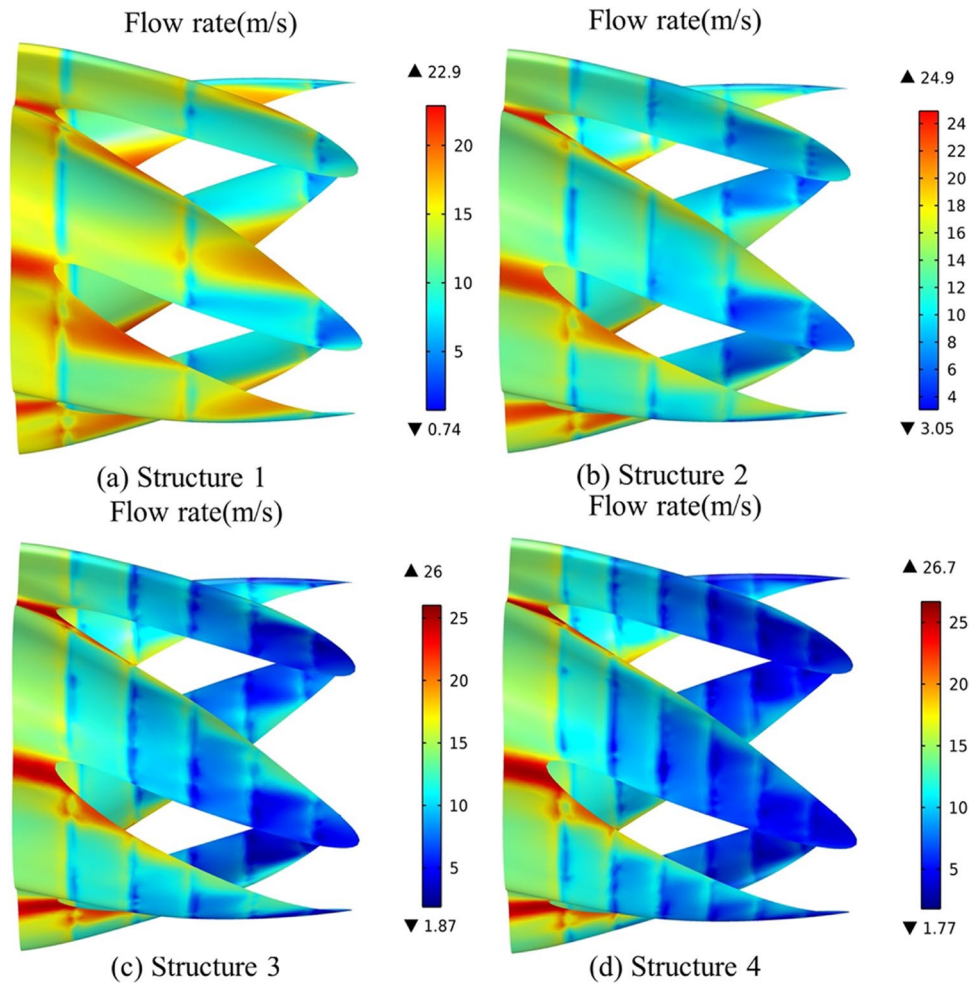


Fig. 8 Cloud plot of electrolyte flow rate distribution in the machining area of the six-tooth cathode with different structures



electrolyte converges to the top of the working tooth and the large end of the working tooth under the action of pressure. The overall flow of electrolytes in structure 2 is better

than the other three structures, with a maximum flow rate of 24.9 m/s and a minimum flow rate of 3.05 m/s, while the maximum flow rate in structure 1 is 22.9 m/s and a minimum

flow rate of 0.74 m/s. This indicates that a small number of booster tanks will have a poor effect on the flow rate of electrolytes in the gap model, and the area with a small minimum flow rate is very prone to The cathode will be burnt when the minimum flow rate is too small. Structure 4 and structure 3 have a low flow rate improvement compared to structure 2, 26 m/s and 26.7 m/s, respectively, but the minimum flow rate is lower compared to structure 2, 1.87 m/s and 1.77 m/s, respectively, which is mainly due to the excessive number of booster tanks, resulting in the influence of the electrolyte flowing out of the machining gap, causing the electrolyte flow interference phenomenon, resulting in the loss of kinetic energy, which leads to the loss of kinetic energy. Structure 4 and structure 3 have a low minimum electrolyte flow rate.

The flow velocity distribution of the electrolyte in the AB cut-off line at the top of the six-tooth cathode is shown in Fig. 9. From the figure, it can be seen that the minimum flow velocity of the electrolyte in the machining area at the top of the teeth has increased significantly compared to the structure before optimization, and the overall flow velocity is above 13.4 m/s, which can quickly take away the anode dissolution products and air bubbles generated in the machining area, improving machining accuracy and ensuring processing stability. The flow velocity of structure 2, structure 3, and structure 4 at the top of the tooth is the same, while the flow velocity of structure 1 is always fluctuating, which is because the small number of liquid increasing tanks leads to the uneven distribution of the flow field. From the curves of structure 2, structure 3, and structure 4, it can be seen that the flow rates of structure 3 and structure 4 on both sides of the tooth top are quite different and uneven, which indicates that too many booster grooves cause interference and turbulence of the electrolyte, resulting in a decrease in the uniformity of the

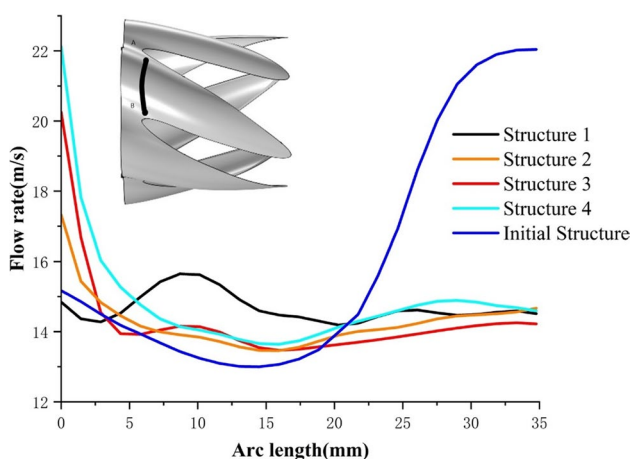


Fig. 9 Flow velocity distribution of the AB cut-off at the top of the six-tooth cathode teeth

electrolyte flow, while the flow rate curve of structure 2 around the tooth top is low, indicating that even increasing the flow rate can ensure the stability of the electrolyte flow of structure 2.

In summary, the cloud diagram of the electrolyte flow velocity distribution in the six-tooth cathode machining area and the cross-sectional flow velocity distribution curve shows that the cathode structure with a structure 2 four-booster bath not only has a fast flow velocity but also a uniform flow field distribution.

4.2.2 Analysis of bubble field simulation results

After optimization of the bubble concentration distribution in the shaped helix deep hole machining region of the cloud diagram shown in Fig. 10, as shown in the figure, after optimization of the gas volume fraction of each structure was reduced, structure 3 and structure 4 are not obvious, the reason for the reduction is due to the structure of structure 3 and structure 4 to increase the liquid tank is too much, the electrolyte produced by the interference interference flow caused by the electrolyte flow uniformity is reduced, so that the change in the volume fraction of the change is not obvious, the structure of structure 1. The reduction rates of gas volume fraction for structure 2 are 14.2% and 28.5%, respectively. The optimized cathode structures with high volume fractions are mainly concentrated at the top of the cathode working teeth and at the cathode big-end joints, and a comparison shows that structure 1, structure 3, and structure 4 all have larger gas volume fractions in the cathode working region, while structure 2 has a lower value of the overall volume fraction in the cathode working region compared to the other three.

As shown in Fig. 11 is a cloud view of the distribution of the gas volume fraction of the AB truncation at the top of the six-tooth cathode tooth, from which it can be seen that the optimized structure 4, which has a significant increase in the volume fraction compared to the initial structure because of the interference perturbation, has a poorer machining quality. The gas volume fraction of structure 3 was not significantly improved compared to the initial structure, and some of the gas volume fraction values of structure 1 were not only higher than those of the initial structure but also higher than those of structure 3. The value of structure 2 is consistently in a slowly increasing state and are smaller than the initial structure as well as other structures, so structure 2 is conducive to improving machining accuracy and ensuring smooth processing.

In summary, through the six-tooth cathode working area electrolyte gas volume fraction distribution cloud diagram

Fig. 10 Gas volume fraction distribution cloud diagram of six-tooth cathode working area with different structures

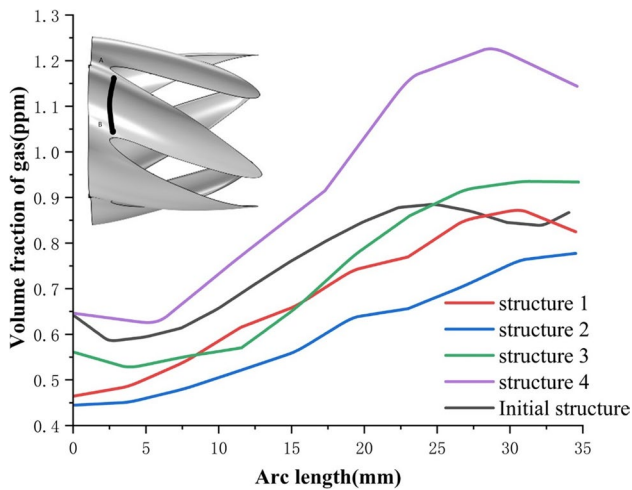
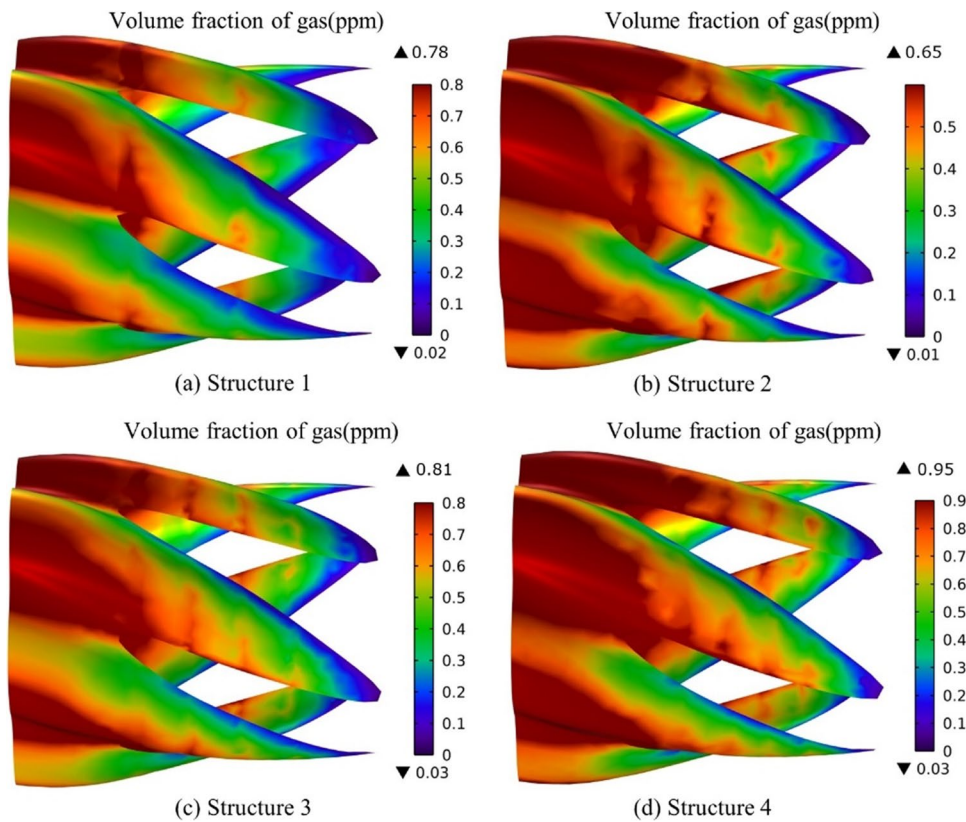


Fig. 11 The gas volume fraction distribution of the AB section of the six-tooth cathode tooth tip

and the truncated line bubble concentration distribution curve, we can see that the electrolyte flow rate of structure 2 cathode structure and the value of gas volume fraction are more reasonable, which is suitable for the machining conditions, and can significantly improve the machining accuracy and machining quality.

5 Tests

5.1 Test systems

The system used in this test is a horizontal electrolytic machine with the workpiece anode connected to a positive power supply and the tool cathode connected to a negative power supply, creating an electrical potential difference between the workpiece and the tool, with the tool cathode controlled by a drawbar control device on the right-hand side for movement. The electrolyte is pressurized by a hydraulic pump and flows at high speed between the workpiece and the tool, carrying away the electrolysis products generated by the workpiece anode and the air bubbles formed by the tool cathode until the machining is completed. The horizontal electrolytic machining process for deep special-shaped hole is shown in Fig. 12 below. The two-dimensional diagram of the tool cathode is shown in Fig. 13.

5.2 Test design

An orthogonal test is used to optimize the multiple objectives so that the optimal results for each value are obtained for the multiple objectives used and to determine the best combination of final machining parameters. An 8% NaNO₃ electrolyte was chosen as the processing electrolyte, and the deviation of the diameter of the large end of the deep

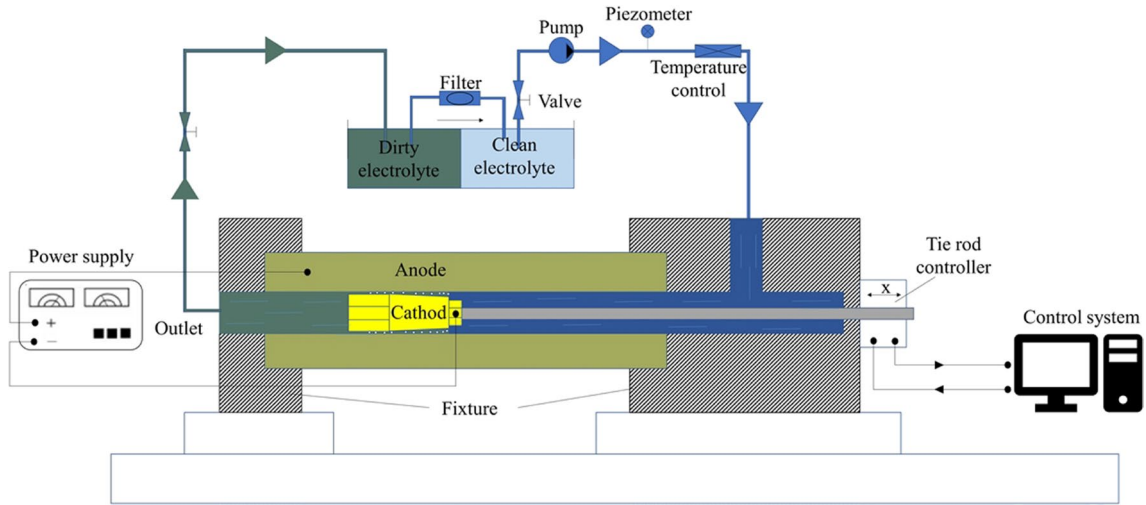


Fig. 12 Schematic diagram of horizontal electrolytic machining process

Fig. 13 Tool cathode two-dimensional diagram

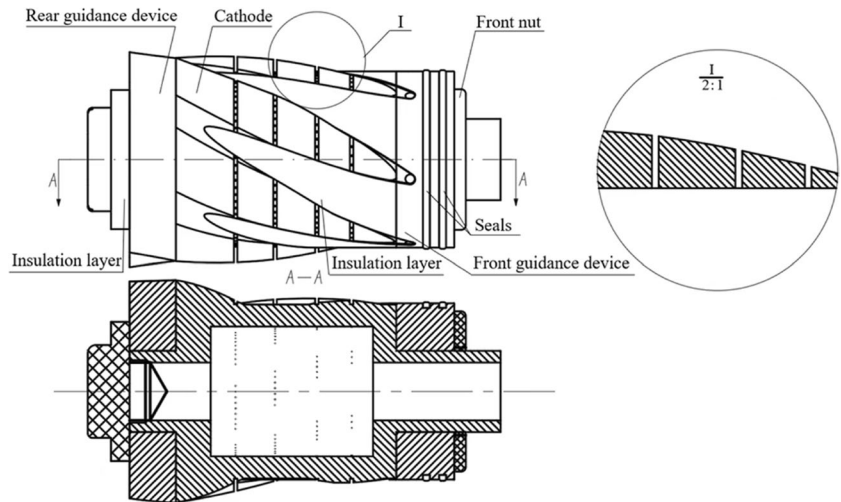


Table 5 Factor levels

Symbol	Control parameters	Level 1	Level 2	Level 3	Level 4
A	Inlet pressure (MPa)	0.4	0.6	0.8	1.0
B	Process voltage (V)	5	8	11	14
C	Duty cycle (%)	30%	35%	40%	45%
D	Feed rate (mm/min)	0.5	0.7	0.9	1.1

special-shaped hole and the surface roughness of the inner wall of the deep special-shaped hole were used as process targets. The inlet pressure, processing voltage, duty cycle, and cathode feed rate used as factors in the process parameters and four levels were set for each process parameter shown in Table 5.

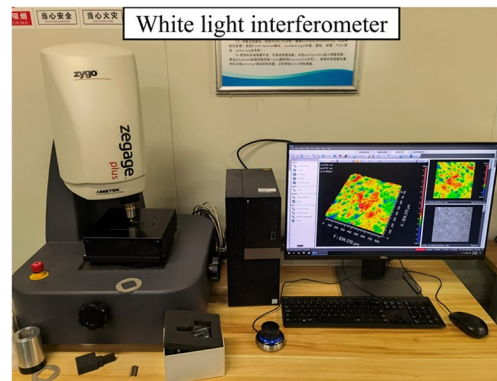


Fig. 14 White light interferometer

5.3 Measuring instruments and methods

The white light interferometer and the three coordinate measuring instrument are used to measure the surface roughness of the inner wall of the deep special-shaped hole and the diameter deviation of the large end of the special-shaped deep hole after the processing test. The white light interferometer is shown in Fig. 14.

The workpiece is sliced using a wire-cut machine at a distance of 60 mm, 120 mm, 180 mm, and 240 mm from the end face of the workpiece, each slice is 6-mm thick, and a CMM is used to measure the coordinates of the diameter of the large end of the deep special-shaped hole at the end face of the slice, as shown in Fig. 15, and the four sets of measured data are averaged. The average value is differenced from the ideal size value and the absolute value is taken as

the final size deviation of the diameter of the large end of the deep special-shaped hole.

We use a white light interferometer to measure the surface roughness of the inner wall surface of the machined deep special-shaped hole and the measured surface roughness values are averaged and solved for as the final surface roughness value.

5.4 Test results

An orthogonal test matrix $L_{16}(4^5)$ with a total of 16 groups of 4 factors and 4 levels, based on the surface roughness of the inner wall of the deep special-shaped hole and the deviation of the diameter of the large end of the deep special-shaped hole for the orthogonal test, and the average value

Fig. 15 Special-shaped deep hole big end diameter coordinate measurement schematic diagram

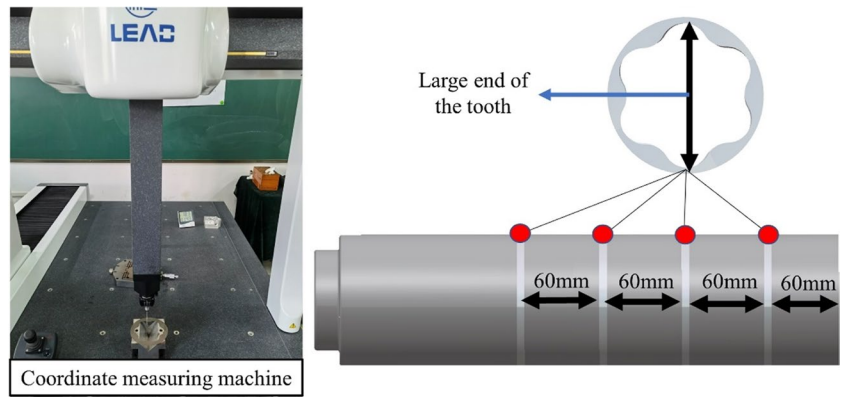


Table 6 Test results

Serial number	Processing parameters				Test measurements	
	A (MPa)	B (V)	C (%)	D (mm/min)	Diameter deviation at large end (mm)	Surface roughness (μm)
1	0.4	5	30	0.5	0.22	0.725
2	0.4	8	35	0.7	0.34	0.834
3	0.4	11	40	0.9	0.15	0.487
4	0.4	14	45	1.1	0.48	1.264
5	0.6	5	35	0.5	0.25	0.641
6	0.6	8	30	0.9	0.43	1.023
7	0.6	11	45	1.1	0.34	0.564
8	0.6	14	40	0.7	0.15	0.357
9	0.8	5	45	0.7	0.17	1.354
10	0.8	8	30	0.9	0.36	0.671
11	0.8	11	40	1.1	0.49	0.489
12	0.8	14	35	0.5	0.51	0.978
13	1.0	5	45	1.1	0.34	0.687
14	1.0	8	40	0.9	0.19	0.486
15	1.0	11	35	0.7	0.33	0.784
16	1.0	14	30	0.5	0.24	0.874

was taken five times for each combination of parameters. The test results are shown in Table 6.

5.5 Optimization of process parameters

The gray correlation method is a method for optimizing parameters when information is incomplete. With the help of the gray correlation, it is possible to measure the influence of the machining parameters used on the deviation of the diameter of the big end of the hexagonal teeth and the surface roughness and thereby find the variable that has the greatest influence on the test results, transforming a problem with multiple objectives into a single problem with comparable indicators and better finding the optimal combination of parameters.

(1) Determining the reference data.

The reference data is generally a set of parameters for which each indicator is optimal, but other reference values can be selected as required. This is noted as $x_0(1), x_0(2), \dots, x_0(n)$.

For this reason, the optimum value for each indicator was chosen as the reference data for this test. Diameter size of the big end of the six teeth is 96 mm and surface roughness 0.6 μm .

(2) Dimensionless indicator data.

The two main methods of using dimensionless processing are as follows:

1. Initialization: dividing the data of the series uniformly by the reference data chosen at the beginning of the experiment. Since the series of the same factor do not differ greatly in magnitude, the values can all be collapsed to around the magnitude of 1 by dividing by the reference data.

$$x_i(k) = \frac{x_i(k)}{x_i(1)}, k = 1, 2, \dots, n; i = 0, 1, 2, \dots, m \quad (8)$$

2. Homogenization: dividing all the data of a sequence by the mean value. Since the mean value of a series of a large order of magnitude is larger, dividing it also normalizes it to around the order of 1.

$$x_i(k) = \frac{x_i(k)}{x_i(1)}, k = 1, 2, \dots, n; i = 0, 1, 2, \dots, m \quad (9)$$

(3) Calculate the absolute value, maximum value, and minimum value of the difference between the index series of the evaluated object and the reference series.

$$|\hat{x}_0(k) - \hat{x}_i(k)|, k = 1, 2, \dots, m; i = 1, 2, \dots, n \quad (10)$$

$$\min = \min(i) \min(k) |\hat{x}_0(k) - \hat{x}_i(k)| \quad (11)$$

$$\max = \max(i) \max(k) |\hat{x}_0(k) - \hat{x}_i(k)| \quad (12)$$

(4) Calculation of correlation coefficients.

$$\epsilon_i(k) = \frac{\min + \rho \max}{|\hat{x}_0(k) - \hat{x}_i(k)| + \rho \max} \quad (13)$$

where ρ is the resolution factor, usually taken as 0.5.

(5) Calculate the correlation.

The mean value of the correlation coefficient between each indicator and the corresponding element of the reference series is calculated separately for each evaluation object, thus reflecting the correlation between each evaluation indicator object and the reference series.

$$r_i = \frac{1}{m} \sum_{k=1}^m \epsilon_i(k) \quad (14)$$

The results of orthogonal tests are shown in Table 7 and the distribution of gray correlation values is shown in Fig. 16; the maximum gray correlation value is obtained for the process parameters of group 3, which has the best machining effect. Specific processing parameters are as follows: inlet pressure 0.4 MPa, processing voltage 11 V, duty cycle 40%, and cathode feed speed 0.9 mm/min. Figure 17 shows the optimal process parameters processing of the processed workpiece to meet the actual production requirements.

6 Conclusion

In this paper, the electrochemical machining technology of internal spiral curved irregular deep hole is studied. The COMSOL software is used to simulate and analyze the gas-liquid two-phase flow field of the initial gap model, optimize the cathode structure, and optimize the processing parameters in combination with the experiment. The processing problem of internal spiral curved irregular deep hole is solved, and the following conclusions are drawn:

(1) The initial cathode structure was optimized by adding different number of liquid-increasing grooves on the tooth surface of the processing tooth, and the gas-liquid two-phase flow field simulation analysis of the initial gap model was carried out for different optimized structures. The results show that the cathode structure with four liquid-increasing grooves has a high overall flow rate of the electrolyte in the processing area, good flow uniformity, low bubble concentration, and small distribution area, and the surface processing quality and accuracy are guaranteed.

Table 7 Test result data

Serial number	Experimental test value		Number of gray contacts		
	Diameter of large end (mm)	Surface roughness (μm)	Diameter of large end (mm)	Surface roughness (μm)	Gray correlation
1	96.22	0.725	0.85274	0.822709	0.837725
2	96.34	0.834	0.680766	0.675941	0.678353
3	96.15	0.487	1.0001185	0.8428572	0.921488
4	96.48	1.264	0.5511004	0.396734	0.473917
5	96.25	0.641	0.8020847	0.9880383	0.895061
6	95.57	1.023	0.5913253	0.5162501	0.553788
7	96.34	0.564	0.6807658	1	0.840383
8	96.15	0.357	1	0.6661291	0.833065
9	95.83	1.354	0.9530568	0.3651636	0.65911
10	96.36	0.671	0.658628	0.921875	0.790251
11	96.49	0.489	0.5437033	0.8463115	0.695007
12	95.49	0.978	0.5294893	0.5470199	0.538255
13	95.66	0.687	0.6807658	0.8900862	0.785426
14	96.19	0.486	0.9102251	0.8411406	0.875683
15	96.33	0.784	0.6924024	0.7361854	0.714294
16	96.24	0.874	0.8182876	0.6344087	0.726348

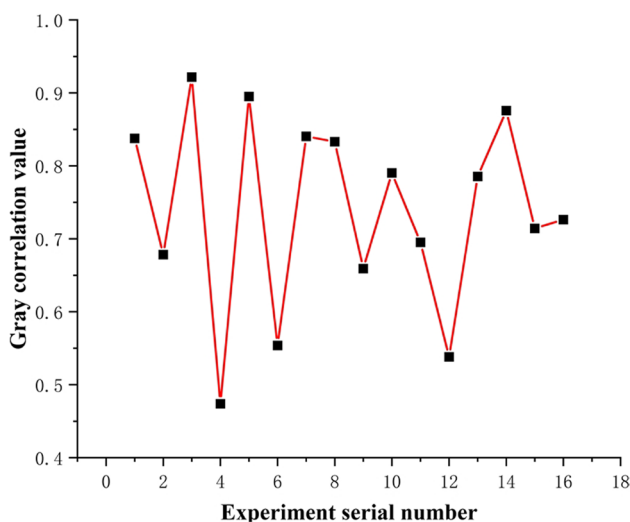


Fig. 16 Line graph of gray correlation values

(2) In the orthogonal test on the machining parameters of electrolytic machining, using gray correlation analysis to optimize the machining parameters, the best machining process parameters are inlet pressure 0.4 MPa, machining voltage 11 V, duty cycle 40%, and cathode feed rate 0.9 mm/min. Under this parameter, the diameter deviation of the large end of the deep special-shaped hole is 0.15 mm, the surface roughness is 0.487 μm, and the processing effect is good. The processing efficiency is good, and the processing precision of the parts meets the product requirements.



Fig. 17 Slicing diagram of workpiece after processing

Author contribution Jianli Jia: paper writing and proofreading of paper content. Yougui Wei: paper writing, data compilation, and translation of papers. Baoji Ma: paper framework construction and paper writing guidance. Jiang Xu: simulation, figure production, paper translation, and proofreading. Yajing Hao: paper typesetting and format modification.

Funding This study has been supported by the Key R&D Project of Shaanxi Provincial Department of Science and Technology (2023-YBGY-186), Shaanxi Province Special Processing Key Laboratory Open Fund Project (SXTZKFJJ202001), and Key R&D Project of Shaanxi Provincial Department of Science and Technology (2019GY-122).

Data availability The data used to support the findings of this study are available from the corresponding author upon request.

Declarations

Consent for publication All authors agree to submit and publish this manuscript in The International Journal of Advanced Manufacturing Technology as a full-length article.

Conflict of interest The authors declare no competing interests.

Ethics approval Because the research of this paper belongs to the field of electrochemical machining, the research content of this paper does not involve ethical issues.

Consent to participate All authors agree to participate in this manuscript.

References

- Ren H (2023) Research on deep hole machining technology in mechanical processing. *Papermaking Equip Mater* 52(04):88–90. <https://doi.org/10.16621/j.cnki.issn1001-0599.2020.04D.83>
- Zhang CL, Chen KZ, Xia X (2018) Experiment and analysis of machining quality of ultra-long deep hole machining of the main body of a smoking gun. *China Strategic Emerg Industries* 12:190. <https://doi.org/10.19474/j.cnki.10-1156/f.003555>
- Guo LW, Li BX, Peng Q (2024) Design and experimental study of composite tool for deep hole machining of fuel regulator shell. *Aeronautical Manufacturing Technology* 1-6 <http://kns.cnki.net/kcms/detail/11.4387.V.20231230.1152.002.html>
- Xing QX, Gao X, Zhang QH (2022) Effects of processing parameters on electrode loss of micro-EDM milling with spiral electrode. *Int J Adv Manuf Technol* 121:5–6. <https://doi.org/10.1007/S00170-022-09598-Y>
- Xu C, Yuan XM, Guan YY (2022) Application and development trend of ultrasonic machining technology. *Metal Working (Metal Cutting)* 091–6. <https://doi.org/10.16107/j.cnki.mmte.2020.1109>
- Li JQ et al (2022) Electrochemical dissolution behavior of Ti6Al4V alloy: effect of microstructure and processing method. *J Mater Process Tech* 307. <https://doi.org/10.1016/J.JMATP.ROTEC.2022.117646>
- Kumar A, Pabla BS (2021) Review on optimized process parameters of electrochemical machining and its variants. *Materials Today: Proceedings* 46(P20). <https://doi.org/10.1016/J.MATPR.2021.01.807>
- Xurong Z, Yongfeng J, Weiming G et al (2021) Optimisation of process parameters for electrochemical machining of a curved hole. *Int J Electrochem Sci* 16(8). <https://doi.org/10.27029/d.cnki.ggdgu.2022.000288>
- Tang L, Feng X, Wang C (2019) Research on electrochemical machining technology of special-shaped internal spiral deep hole with large length-diameter ratio. *Special Machining Branch of China Society of Mechanical Engineering. The 18 th National Non-traditional Machining Academic Conference Proceedings (Abstract). Shaanxi Provincial Key Laboratory of Non-traditional Machining, Xi 'an University of Technology* 1. <https://doi.org/10.26914/c.cnkiyh.2019.068632>
- Rahman Md, Zishanur DA, Kumar, Somnath C (2020) Effects of balance electrode in deep micro-holes drilling in nickel plate through μ ECM process using H₂SO₄ electrolyte. *Materials Today: Proceedings* 43. prepublsh. <https://doi.org/10.1016/j.matpr.2020.09.180>
- Rakhimyanov K, Vasilevskaya S, Rakhimyanov K (2020) Controlling the forming of deep holes of a small diameter by mixed piercing based on a system analysis of the processes in the inter-electrode gap. *Materials Today: Proceedings*.prepublsh. <https://doi.org/10.1016/j.matpr.2020.08.236>
- Prakash J, Gopalakannan S (2020) Teaching-learning-based optimization coupled with response surface methodology for micro electrochemical machining of aluminium nanocomposite. *Silicon* 13:409–432. <https://doi.org/10.1007/s12633-020-00434-0>
- Zhang C (2020) Cathodic modification, numerical simulation and experimental investigation on electrochemical machining for the small inner-walled ring groove. *Int J Electrochem Sci* 15(4). <https://doi.org/10.20964/2020.02.56>
- Yuan K et al (2022) Design and optimization of cathode for ECM of high-speed steel roll material based on multi-physics field coupling analysis. *Int J Adv Manuf Technol* 121:11–12. <https://doi.org/10.1007/S00170-022-09718-8>
- Pratik R, Shah SS, Pande (2020) Computer aided tool design for micro-ECM. *Int J Precision Technol* 9(1). <https://doi.org/10.1504/ijptech.2020.10031885>
- Chen Y, Zhou X, Chen P, Wang Z (2020) Electrochemical machining gap prediction with multi-physics coupling model based on two-phase turbulence flow. *Chin J Aeronaut* 33(3). <https://doi.org/10.1016/j.cja.2019.03.006>
- Shen MQ et al (2019) Experimental study on electrolytic machining of small tapered tapered holes. *Mech Des* 3607:7–13. <https://doi.org/10.13841/j.cnki.jxsj.2019.07.002>
- Feng W et al (2020) Electrochemical machining of a rhombus hole with synchronization of pulse current and low-frequency oscillations. *J Manuf Process* 57. <https://doi.org/10.1016/j.jmapro.2020.06.014>
- Tim VDV, Bob R, Andreas K et al (2021) A novel approach for the efficient modeling of material dissolution in electrochemical machining. *Int J Solids Struct.* 229 <https://doi.org/10.1016/j.ijsolstr.2021.111106>
- Yin FH, Jiang LW, Xiao HX, He YF, Gan WM (2018) Experimental electrolytic machining of hexagonal-shaped holes and process optimization [J]. *Manuf Autom* 40(02):60–64. <https://doi.org/10.3969/j.issn.1009-0134.2018.02.016>
- Jia, Jianli et al (2022) Analysis of flow field for ECM square deep hole with two-section square cone combination cathode. *Int J Adv Manuf Technol* 121:7–8. <https://doi.org/10.1007/S00170-022-09670-7>

Publisher's note Springer Nature remains neutral with regard to jurisdictional claims in published maps and institutional affiliations.

Springer Nature or its licensor (e.g. a society or other partner) holds exclusive rights to this article under a publishing agreement with the author(s) or other rightsholder(s); author self-archiving of the accepted manuscript version of this article is solely governed by the terms of such publishing agreement and applicable law.